Meas. Sci. Technol. **21** (2010) 065801 (10pp) doi:10.1088/0957-0233/21/6/065801

Stochastic magnetic measurement model for relative position and orientation estimation

H M Schepers[1,2] **and P H Veltink**[1]

[1] Institute for Biomedical Technology (BMTI), University of Twente, PO Box 217, 7500 AE Enschede, The Netherlands
[2] Xsens Technologies B.V., Pantheon 6a, 7521 PR Enschede, The Netherlands

Received 26 January 2010, in final form 15 March 2010
Published 28 April 2010
Online at stacks.iop.org/MST/21/065801

Abstract
This study presents a stochastic magnetic measurement model that can be used to estimate relative position and orientation. The model predicts the magnetic field generated by a single source coil at the location of the sensor. The model was used in a fusion filter that predicts the change of position and orientation by integration of acceleration and angular velocity measured by inertial sensors. If the uncertainty associated with the position and orientation exceeds a predefined threshold, the filter decides to perform a magnetic update by actuating only that coil which results in the largest reduction of the uncertainty. The difference between the actual magnetic measurement and the prediction of the measurement was used to reduce the drift caused by integration of acceleration and angular velocity. The model is accurate as confirmed by the small rms differences between validation measurements and predictions of the magnetic field using the model. The use of a linearized version of the measurement model for the fusion filter and the appearance of a ferromagnetic object in the vicinity of the source or sensor were defined as two sources of error that may lead to divergence of the fusion filter. Both sources of error were analyzed and it appeared that the linearized model introduces errors which generally increase for sensor locations near the source. Moreover, it appeared that a ferromagnetic object influences the measurements only if it is located near or between the source and the sensor.

Keywords: magnetic sensing, inertial sensing, extended Kalman filter, human motion tracking

1. Introduction

Human motion tracking comprises the reconstruction of position and orientation of body segments. Several methods exist for the estimation of positions and orientation based on different principles, for example optical, magnetic or acoustic. A common drawback of the existing measurement systems is their restriction to a laboratory environment. A solution to overcome this common drawback is the use of inertial sensors (accelerometers and gyroscopes). The change of position and orientation can be estimated by integration of acceleration and angular velocity, respectively. However, since the sensor signals are rather noisy and can have a fluctuating offset, integration of these signals involved in estimation of orientation and position change introduces integration drift. This drift can be limited by using suitable estimation algorithms [1–4], initial and final conditions and limiting the integration time [5, 6]. Still, a stable, robust and ambulatory solution is desired, especially for the estimation of relative position of body segments since the starting position is unknown.

A commonly used solution is to fuse inertial measurements with an aiding system. An example is the use of GPS measurements [7, 8], but the accuracy is limited partly due to possible loss or degradation of the GPS signal, especially for relative positions between body segments. Other examples are the use of an acoustic time-of-flight measurement system [9], or an optical [10], or a magnetic position and orientation tracking system [11]. However, these systems are commonly fixed to a laboratory environment. Recently, it was proposed

to fuse inertial sensing with ultra-wide band positioning [12]. An advantage of magnetic tracking compared to ultra-wide band or acoustic tracking is that the human body is transparent for the field applied. Compared to GPS tracking, magnetic tracking does not suffer from the mentioned loss or degradation of the signal, although it is sensitive to disturbances caused by for example ferromagnetic material. Summarizing, it can be concluded that the combination of an inertial measurement system and an ambulatory magnetic tracking system that can minimize errors due to magnetic disturbances may be a good choice to estimate relative positions and orientations of body segments.

An ambulatory magnetic position and orientation measurement system was previously proposed by Roetenberg *et al* [13]. A major advantage over commercially available systems, like Fastrak (Polhemus) and Flock of Birds (Ascension Technology) as used by Emura and Tachi [11], is that the magnetic source is worn on the body, which means measurements can be performed during everyday life. Moreover, since the ranges to be covered are generally smaller compared to the available systems, the coil dimensions can be reduced. A drawback is that, besides the movement of the sensor, the movement of the source needs to be estimated. In another study [14], the measurement system was fused with an inertial sensor system using a complementary Kalman filter structure to correct for the integration drift, and to reduce errors related to magnetic disturbances. Although the results were promising, the method needs to be improved in several aspects. The estimation algorithm [15, 16], based on a magnetic dipole approximation of the source, requires all three source coils to be actuated at every update, while the update rate is fixed and pre-assigned by the user. Moreover, the calculations did not involve a stochastic measurement model required for sensor fusion applying optimal estimation methods. Such a stochastic measurement model would also allow for an optimal choice of the activation levels. Also, the source consisted of three coils which need to be mounted orthogonally and share the same origin. An algorithm using two source coils was proposed by Paperno *et al* [17], but still the two coils needed to be mounted orthogonally and to share the same origin.

In order to apply the ambulatory magnetic position and orientation estimation system more generally, an estimation method is needed which is not based on the dipole approximation and does not require the source coils to be mounted orthogonally or to share the same origin. A fusion filter was designed [18] that combines inertial and magnetic sensing to estimate relative position and orientation of a remote sensor with respect to the source. The system consists of three source coils, but the filter decides to actuate only a single coil when needed and chooses the coil which results in the largest reduction of the uncertainty based on the stochastic model of a single source coil. The objective of this study is to present and validate this stochastic measurement model that predicts the magnetic measurement based on an estimation of the relative position and orientation of the remote sensor with respect to the source. The accuracy of the measurement model is validated using a source coil and a remote sensor at known position and orientation. Moreover, the influence of a ferromagnetic object in the vicinity of the measurement system is analyzed.

2. Methods

2.1. Sensor fusion

The measurement model proposed and evaluated in this paper was used in a fusion filter to estimate relative positions and orientations of a remote sensor with respect to a source [18]. The source consists of one or more coils mounted in a known configuration which can be actuated independently. The remote sensor consists of an inertial sensor (3D accelerometer and 3D gyroscope) and a 3D magnetometer. The inertial sensor is used to predict the change of position and orientation by integration of the sensor signals. Since integration of noisy signals with a fluctuating offset introduces drift, magnetic updates are used to reduce the drift. The fusion filter compares the measurements to a prediction of the measurements using a stochastic magnetic measurement model and updates the estimates of position and orientation based on the difference between prediction and measurement. In general, a stochastic measurement model is described by

$$\boldsymbol{y} = \boldsymbol{h}(\boldsymbol{x}) + \boldsymbol{v}, \tag{1}$$

where $\boldsymbol{h}(\boldsymbol{x})$ denotes the nonlinear function which maps the state vector $\boldsymbol{x}$ to the measurement vector $\boldsymbol{y}$. The additive measurement noise is denoted by $\boldsymbol{v}$ with covariance $\mathbf{R}_v$.

The process of predicting and updating the estimation of a state variable is schematically depicted in figure 1. In between magnetic updates, the estimated uncertainty of a state variable σ_x increases due to the drift caused by integration of inertial sensor signals. An actuation is required if the estimated uncertainty reaches a predefined maximum $\sigma_{x,\max}$. Only the coil yielding the largest uncertainty reduction is actuated and the current applied is chosen such that the uncertainty decreases to a predefined minimum $\sigma_{x,\min}$.

A schematic overview of a configuration with a coil around the z-axis is depicted in figure 2. The coil frame is denoted by Ψ_c and the sensor frame by Ψ_s. The true state vector consists of the relative position and orientation of the sensor frame with respect to the source frame: $\boldsymbol{p}_s^c$ and θ_s^c, respectively. It is chosen to use a fusion filter that operates on the errors of the state $\delta\boldsymbol{x}$, being the difference between the true state $\boldsymbol{x}$ and the estimated state $\hat{\boldsymbol{x}}$. Let $\hat{\boldsymbol{p}}_s^c$ be the estimated relative position and $\hat{\mathbf{R}}_s^c$ be the relative orientation of the sensor with respect to the coil expressed as a rotation matrix. The columns of $\hat{\mathbf{R}}_s^c$ are the unit axes of the frame Ψ_s expressed in the frame Ψ_c: $\hat{\mathbf{R}}_s^c = \begin{pmatrix}\hat{\boldsymbol{X}}_s^c & \hat{\boldsymbol{Y}}_s^c & \hat{\boldsymbol{Z}}_s^c\end{pmatrix}$. The estimated states are related to the true states by

$$\begin{aligned}\hat{\boldsymbol{p}}_s^c &= \boldsymbol{p}_s^c + \delta\boldsymbol{p}\\ \hat{\mathbf{R}}_s^c &= \mathbf{R}_s^c\delta\mathbf{R} \approx \mathbf{R}_s^c(\mathbf{I} + \tilde{\delta\theta}),\end{aligned} \tag{2}$$

with $\mathbf{I}$ the identity matrix, $\delta\boldsymbol{p}$ the position error and $\delta\theta$ the orientation error. Consequently, the error state is equal to $\delta\boldsymbol{x} = (\delta\boldsymbol{p}\ \delta\theta)^T$. The tilde operator ($\tilde{}$) defines the matrix form of the standard vector product:

$$\tilde{\delta\theta} = \begin{pmatrix} 0 & -\delta\theta_z & \delta\theta_y \\ \delta\theta_z & 0 & -\delta\theta_x \\ -\delta\theta_y & \delta\theta_x & 0 \end{pmatrix}. \tag{3}$$

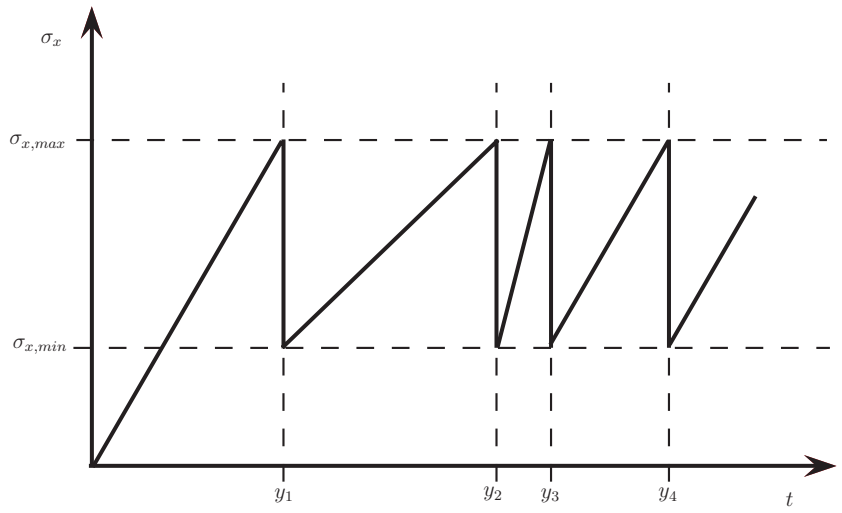

Figure 1. Schematic overview of the reduction of the uncertainty associated with a state variable σ_x by fusion with measurements y. The time interval between updates is not fixed since the filter updates only when the uncertainty exceeds a predefined threshold ($\sigma_{x,\max}$).

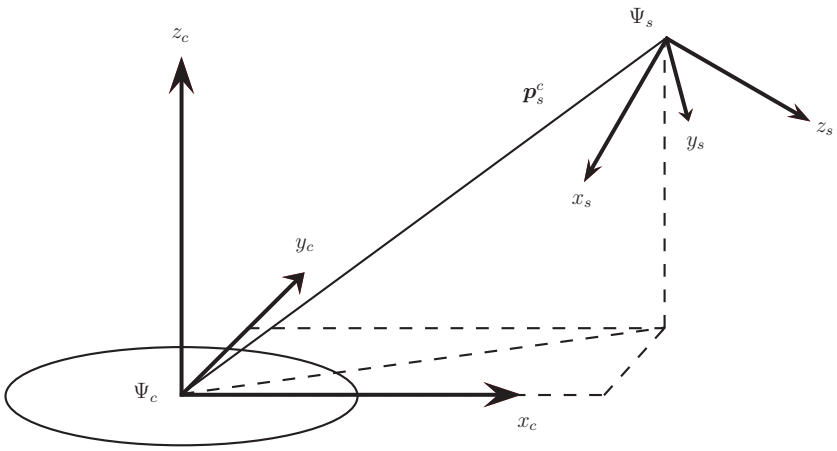

Figure 2. Schematic overview of a configuration with a coil around the z-axis (frame Ψ_c) and a remote sensor (Ψ_s).

To estimate the reduction of the state covariance, we exploit the equations of an extended Kalman filter (EKF). Let $\mathbf{P}_k$ be the covariance associated with the state $\delta\boldsymbol{x}_k$ at the time instant k. For a Kalman filter, a linear update rule is specified that calculates the Kalman gain $\mathbf{K}_k$ which is used to transform the difference between actual and predicted measurements from measurement space to state vector space:

$$\begin{aligned} \delta\boldsymbol{x}_k &= \mathbf{K}_k \delta\boldsymbol{y}_k \\ \mathbf{P}_k &= (\mathbf{I} - \mathbf{K}_k\mathbf{H}_k)\mathbf{P}_k^- \\ \delta\boldsymbol{y}_k &= \hat{\boldsymbol{y}}_k^- - \boldsymbol{y}_k \\ \mathbf{K}_k &= \mathbf{P}_k^-\mathbf{H}_k^T\left(\mathbf{H}_k\mathbf{P}_k^-\mathbf{H}_k^T + \mathbf{R}_v\right)^{-1}, \end{aligned} \tag{4}$$

where $\mathbf{H}_k$ denotes a linearized version of the measurement model $\boldsymbol{h}(\boldsymbol{x})$. It should be noted that a minus superscript $(\,)^-$ denotes the *a priori* estimation of a variable. Thus, by using the linearized measurement model $\mathbf{H}_k$, the *a posteriori* covariance $\mathbf{P}_k$ is obtained. Moreover, by calculating the reduction of the state uncertainty for each of the coils that can be actuated, the filter can decide which coil needs to be actuated such that the reduction of the state uncertainty is highest.

The nonlinear stochastic measurement model is derived in section 2.2 and validated by experiments that are described in section 2.4. The derivation of the linearized measurement is shown in section 2.3. Two sources of error can be defined which may lead to divergence of the fusion filter. The first source of error is the use of a linearized approximation for the nonlinear measurement model to update the state and covariance (4). The linear approximation introduces errors that are not covered by the update equations and can cause the filter to diverge. Another source of error is the appearance of ferromagnetic objects in the vicinity of the source or the sensor, which can cause the measured magnetic field to deviate from the generated magnetic field. The filter will attribute such a deviation to an error of the state which yields an incorrect state update that may lead to divergence of the filter as well. Both sources of errors will be analyzed and discussed in the following sections.

2.2. Measurement model

The estimated measurement vector $\hat{\boldsymbol{y}}$ is given by the magnetic field generated by the source coil at the location of the sensor $\hat{\boldsymbol{B}}^c(\hat{\boldsymbol{p}}_s^c)$, expressed in sensor coordinates [18]:

$$\hat{\boldsymbol{y}} = \boldsymbol{h}(\hat{\boldsymbol{x}}) = \hat{\boldsymbol{B}}^s = \left(\hat{\mathbf{R}}_s^c\right)^T \hat{\boldsymbol{B}}^c\left(\hat{\boldsymbol{p}}_s^c\right). \tag{5}$$

The expression for the magnetic field $\hat{\boldsymbol{B}}^c(\hat{\boldsymbol{p}}_s^c)$ at the location of the sensor generated by the actuated source coil is derived by applying the Biot–Savart law [19], resulting in

$$\hat{\boldsymbol{B}}^c\left(\hat{\boldsymbol{p}}_s^c\right) = \frac{\mu_0 N I}{2\pi\sqrt{\left(\sqrt{\hat{p}_x^2+\hat{p}_y^2}+b\right)^2+\hat{p}_z^2}} \times \begin{pmatrix} \frac{\hat{p}_x\hat{p}_z}{\hat{p}_x^2+\hat{p}_y^2}\left(-K(k)+\frac{b^2+\hat{p}_x^2+\hat{p}_y^2+\hat{p}_z^2}{(\sqrt{\hat{p}_x^2+\hat{p}_y^2}-b)^2+\hat{p}_z^2}E(k)\right) \\ \frac{\hat{p}_y\hat{p}_z}{\hat{p}_x^2+\hat{p}_y^2}\left(-K(k)+\frac{b^2+\hat{p}_x^2+\hat{p}_y^2+\hat{p}_z^2}{(\sqrt{\hat{p}_x^2+\hat{p}_y^2}-b)^2+\hat{p}_z^2}E(k)\right) \\ K(k)+\frac{b^2-\hat{p}_x^2-\hat{p}_y^2-\hat{p}_z^2}{(\sqrt{\hat{p}_x^2+\hat{p}_y^2}-b)^2+\hat{p}_z^2}E(k) \end{pmatrix}, \tag{6}$$

with μ_0 the magnetic permeability of vacuum ($4\pi \times 10^{-7}$ T m A^{-1}), N the number of windings, I the current applied, b the radius of the coil, and

$$\begin{aligned} k &= \sqrt{\frac{4b\sqrt{\hat{p}_x^2+\hat{p}_y^2}}{\left(\sqrt{\hat{p}_x^2+\hat{p}_y^2}+b\right)^2+\hat{p}_z^2}} \\ K(k) &= \int_0^{\pi/2} \frac{1}{\sqrt{1-k^2\sin^2\phi}}\,\mathrm{d}\phi \\ E(k) &= \int_0^{\pi/2} \sqrt{1-k^2\sin^2\phi}\,\mathrm{d}\phi. \end{aligned} \tag{7}$$

It should be noted that the indices $()_s^c$ have been omitted for readability. Solving the elliptic integrals $E(k)$ and $K(k)$ for every time step can be rather time consuming. The expression for the magnetic flux density (6) can be simplified by assuming that the point of interest satisfies $\sqrt{\hat{p}_x^2+\hat{p}_y^2+\hat{p}_z^2} \gg b$, which means that the coil is viewed as a magnetic dipole resulting in

$$\hat{\boldsymbol{B}}^c\left(\hat{\boldsymbol{p}}_s^c\right) = \frac{\mu_0 N I b^2}{4\left(\hat{p}_x^2+\hat{p}_y^2+\hat{p}_z^2\right)^{\frac{5}{2}}} \begin{pmatrix} 3\hat{p}_x\hat{p}_z \\ 3\hat{p}_y\hat{p}_z \\ 2\hat{p}_z^2-\hat{p}_x^2-\hat{p}_y^2 \end{pmatrix}. \tag{8}$$

2.3. Linearized measurement model

In order to determine the reduction of the uncertainty associated with the state and to determine which coil has to be actuated, the first-order linearized measurement model (Jacobian) needs to be derived. The Jacobian $\mathbf{H}$, consisting of the partial derivatives of the function $\boldsymbol{h}(\hat{\boldsymbol{x}})$ with respect to the error state $\delta\boldsymbol{x}$, is given by

$$\mathbf{H} = \begin{pmatrix} \frac{\partial\hat{\boldsymbol{B}}^s}{\partial\delta\boldsymbol{p}} & \frac{\partial\hat{\boldsymbol{B}}^s}{\partial\delta\theta} \end{pmatrix} = \begin{pmatrix} \left(\hat{\mathbf{R}}_s^c\right)^T\frac{\partial\hat{\boldsymbol{B}}^c}{\partial\delta\boldsymbol{p}} & \frac{\partial\left(\hat{\mathbf{R}}_s^c\right)^T}{\partial\delta\theta}\hat{\boldsymbol{B}}^c \end{pmatrix}. \tag{9}$$

The partial derivatives of the estimated field with respect to the position error $\left(\left(\hat{\mathbf{R}}_s^c\right)^T\frac{\partial\hat{\boldsymbol{B}}^c}{\partial\delta\boldsymbol{p}}\right)$ result in rather lengthy and complicated expressions for the analytical model and are therefore not shown. For the dipole approximation of the magnetic field, the results are more straightforward and as an example the partial derivative with respect to the first error state is given by

$$\left(\hat{\mathbf{R}}_s^c\right)^T\frac{\partial\hat{\boldsymbol{B}}^c}{\partial\delta p_x} = \left(\hat{\mathbf{R}}_s^c\right)^T\frac{\mu_0 N I b^2}{4\left(\hat{p}_x^2+\hat{p}_y^2+\hat{p}_z^2\right)^{\frac{7}{2}}} \times \begin{pmatrix} -12\hat{p}_x^2\hat{p}_z+3\hat{p}_y^2\hat{p}_z+3\hat{p}_z^3 \\ -15\hat{p}_x\hat{p}_y\hat{p}_z \\ 3\hat{p}_x^3+3\hat{p}_x\hat{p}_y^2-12\hat{p}_x\hat{p}_z^2 \end{pmatrix}. \tag{10}$$

The partial derivatives of the estimated field to the orientation are given by

$$\begin{aligned} \frac{\partial\left(\hat{\mathbf{R}}_s^c\right)^T}{\partial\delta\theta}\hat{\boldsymbol{B}}^c &= \frac{\partial}{\partial\delta\theta}\left(\mathbf{R}_s^c\delta\mathbf{R}\right)^T\hat{\boldsymbol{B}}^c = \frac{\partial}{\partial\delta\theta}\left(\mathbf{I}-\delta\tilde{\theta}\right)\left(\mathbf{R}_s^c\right)^T\hat{\boldsymbol{B}}^c \\ &= \frac{\partial}{\partial\delta\theta}\left(\hat{\boldsymbol{B}}^s+\tilde{\hat{\boldsymbol{B}}}^s\delta\theta\right) = \tilde{\hat{\boldsymbol{B}}}^s, \end{aligned} \tag{11}$$

with $\hat{\boldsymbol{B}}^s$ the estimation of the magnetic field generated by the source at the location of the sensor expressed in sensor coordinates.

2.4. Experimental methods

To evaluate the performance of the stochastic magnetic measurement model, several aspects of the stochastic measurement model were validated by experiments. The measurement setup consisted of an x–y positioning table with a single coil around the x-axis at the origin as shown in figure 3. It should be noted that the z-position was not varied during the measurements, since the magnetic field generated by the coils is axially symmetric. Moreover, the orientation of the sensor was not changed during the measurements as this will not affect the strength of the magnetic field, but the distribution of the individual components only. An error in the estimation of orientation will, however, affect the update of the states calculated by the fusion filter. The measurements were done using the magnetometer (thin film magnetoresistive) of a MTx sensor (Xsens Technologies B.V.). The signals were acquired at a sample rate of 100 Hz. The noise level of the sensors σ_v was determined to be 0.3 mG. During the actuation, the magnetometer measures the sum of the Earth's magnetic field and the actuated magnetic field. Pulse values were extracted by detecting sudden changes on the magnetometer signal after a magnetic actuation, and subtracting the signal without actuation from the signal with actuation. The coil was a circular coil with 50 windings and a radius of 0.055 m. The coil was actuated each second at a current of 0.91 A using a pulse width of 100 ms (ten samples).

The experiment consisted of three parts. First, the accuracy of the nonlinear measurement model was validated by placing the sensor at known positions and measuring the responses. The positions are indicated by the dots in figure 3 and were chosen to cover the largest part of the magnetic field in the measurement volume. The accuracy was evaluated by comparing the responses to a prediction of the magnetic field at the known magnetic field at the known positions using the nonlinear model. Both the

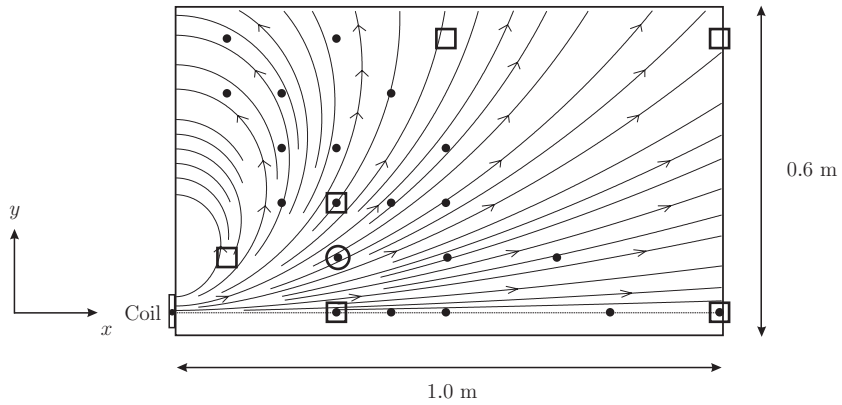

Figure 3. Schematic drawing of the 2D measurement setup with the sensor positions used for validation of the nonlinear measurement model (dots), the linearized model (circle) and the influence of a magnetic disturbance (circle). The positions of the ferromagnetic object are indicated by the squares. The seventh position of the ferromagnetic object ($(x, y) = (2.0, 0.0)$ m) is not shown. The lines with arrows indicate the magnetic field lines generated by the coil.

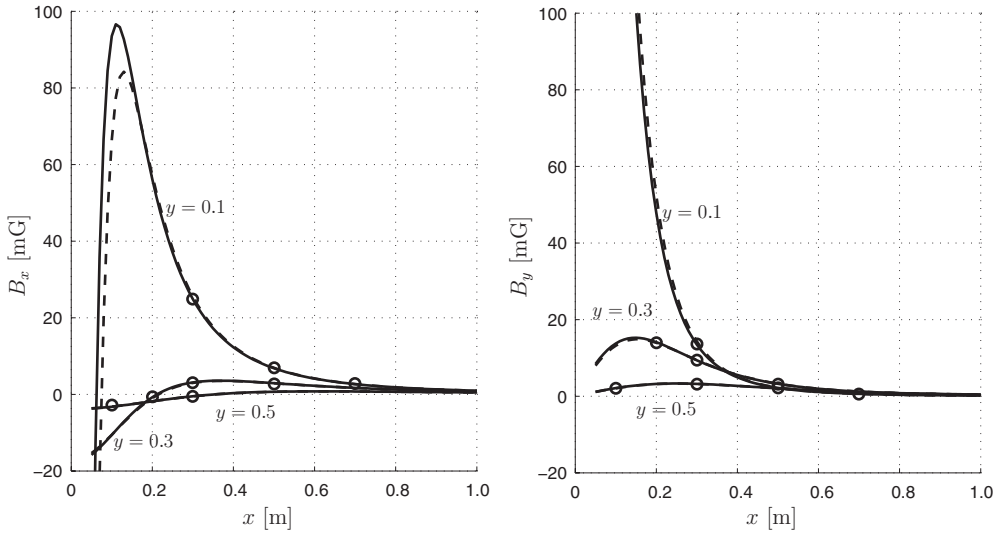

Figure 4. Components (B_x left, B_y right) for the predicted magnetic field (lines) and measured magnetic field (circles) for varying x position at constant y position at an actuation current of 0.91 A. The predictions were made using the analytical model (solid) and the dipole approximation (dashed).

dipole approximation and the analytical model were evaluated. Second, the accuracy of the linearized model was validated by placing the sensor at position $(x, y) = (0.3, 0.1)$ m, as indicated by the circle in figure 3. Subsequently, the position was varied around the initial position in steps of 5 mm in positive x and y directions with a maximum of 5 cm. The accuracy of the change of the magnetic field was evaluated by comparison to the change predicted by the Jacobian using the dipole approximation as well as the analytical model. Third, the influence of a ferromagnetic disturbance was evaluated by placing the sensor at a fixed position ($(x, y) = (0.3, 0.1)$ m, circle in figure 3) and a ferromagnetic object (iron cylinder with a radius and a height of 0.05 m) at several positions around the sensor, as indicated by the squares in figure 3. By comparing the disturbed response at each position of the ferromagnetic object to the undisturbed response, the influence of the disturbance is determined.

3. Results

3.1. Validation of the nonlinear measurement model

For validation of the nonlinear measurement model, the sensor was placed at positions indicated by the dots in figure 3. A comparison between the measured magnetic field components and the predicted magnetic field components for varying x positions and a few constant y positions using the analytical model and the dipole approximation is shown in figure 4. The analytical model is accurate, as confirmed by the rms differences which were calculated as 0.50 ± 0.22 mG (mean $\pm$ standard deviation) for the x direction and 0.14 ± 0.06 mG

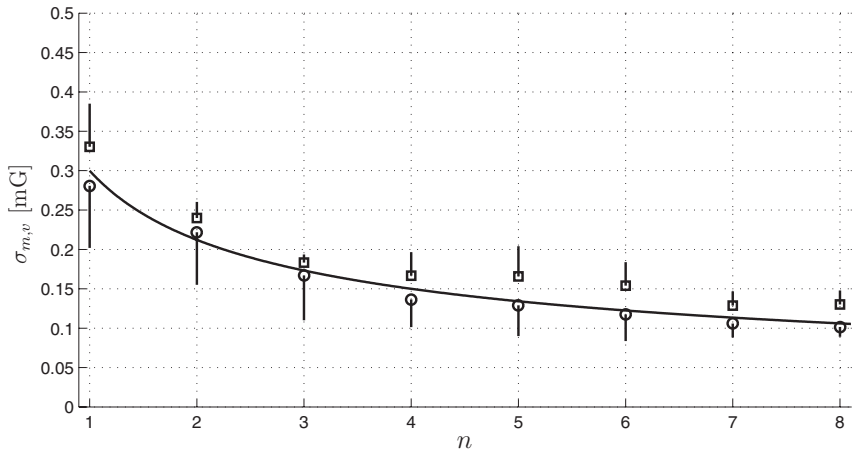

Figure 5. Standard deviation of the sample mean $\sigma_{m,v}$ as a function of the number of samples n used to calculate the mean. The estimated average of $\sigma_{m,v}$ and its standard deviation are indicated by the dots (x: circle, y square) and vertical lines, respectively. It should be noted that the standard deviation is only shown at a single side of the mean for visualization reasons. The solid line indicates the predicted decrease of $\sigma_{m,v}$.

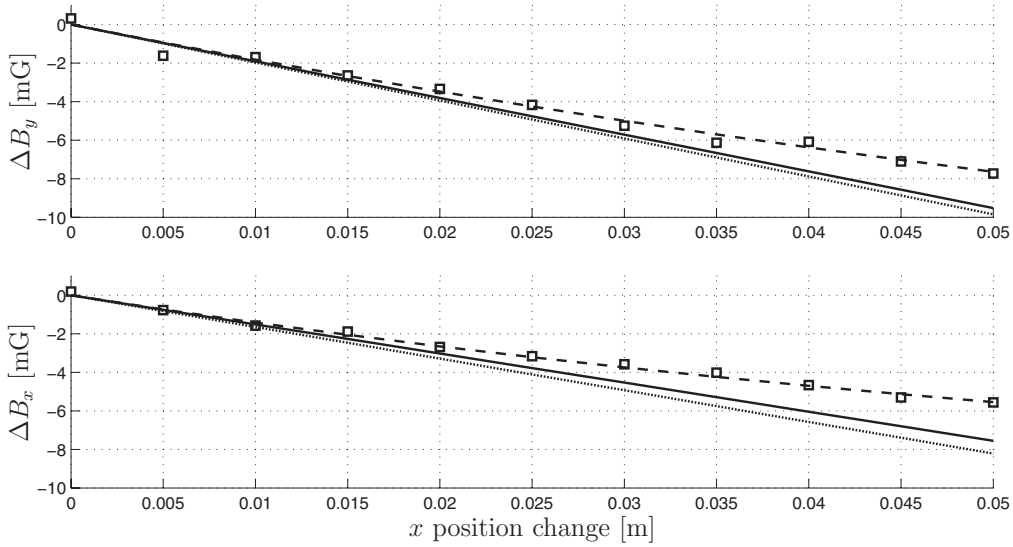

Figure 6. Validation of the Jacobian by comparing the change of the magnetic field for the x direction (top figure) and y direction (bottom figure) due to an increase in positive x position of the sensor starting at $(x, y) = (0.3, 0.1)$ m. The actual field measured by the magnetometer is indicated by the squares, and the prediction using the nonlinear model is indicated by the dashed line. The prediction of the field change using the Jacobian calculated from the analytical model is indicated by the solid line. The prediction of the field change using the Jacobian calculated from the dipole approximation is indicated by the dotted line.

for the y direction. Moreover, the figure clearly indicates the increasing error of the dipole approximation for sensor locations near the source. The rms differences using the dipole approximation were calculated as 0.53 ± 0.27 mG for the x direction and 0.18 ± 0.15 mG for the y direction.

To construct figure 4 and to calculate the rms differences, all samples except the first and the last of each pulse were used for averaging. The first and last samples were not used, because they may have occurred in the rising or falling edge of a pulse. To prevent the magnetic field to change by sensor movement during a pulse, the number of samples should be as small as possible. This will, however, decrease the accuracy which is graphically depicted in figure 5. The figure shows the decrease of the standard deviation of the sample mean $\sigma_{m,v}$ as a function of the number of samples used to calculate the mean. The predicted $\sigma_{m,v}$ (solid line) is calculated by $\sigma_{m,v} = \frac{\sigma_v}{\sqrt{n}}$, with n being the number of samples [20].

3.2. Validation of the linearized measurement model

A comparison of the change of magnetic field components by an increase of the sensor position in the x direction starting at position $(x, y) = (0.3, 0.1)$ m is shown in figure 6. The figure clearly shows the error caused by the linear approximation of the nonlinear field using the Jacobian. As expected, the error increases more when the dipole approximation is used, compared to when the analytical model is used. In order to analyze the errors caused by the use of the linearized

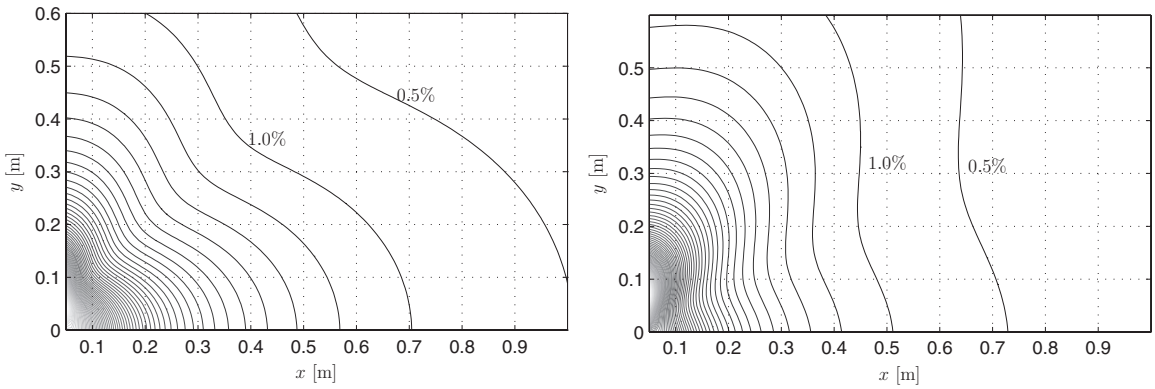

Figure 7. Percentage difference between the magnetic fields estimated by the linearized and nonlinear models for a position uncertainty of 0.03 m in the x direction (left) and y direction (right). Each line indicates an increase of 0.5%.

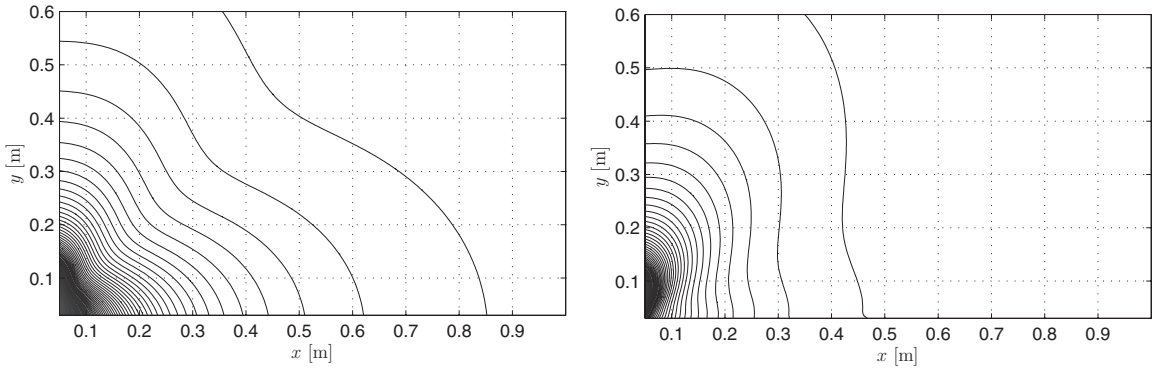

Figure 8. Magnitude of the second-order spatial derivative of the magnetic field to x (left) and y (right), divided by the magnitude of the magnetic field.

measurement model, the percentage difference between the magnetic fields estimated by the linearized and nonlinear models was calculated at a predefined uncertainty of the estimated position for the complete measurement volume (figure 7). The predefined uncertainty, which can be viewed as the position change in figure 6, was chosen to be 0.03 m for the x and y directions as an example. The percentage difference is calculated by dividing the magnitude of the field difference between the linearized model and the nonlinear model at the predefined uncertainty (0.03 m) by the magnitude of the field at the current position. The figure shows an increase in percentage difference due to the use of the linearized model for sensor locations near the source. Since we used a linear approximation of the nonlinear measurement model, the error levels (figure 7) can be viewed as the higher order terms of the Taylor approximation of the nonlinear measurement model, of which the second-order term will be dominant. This is confirmed by the similar shape of the levels in figure 7 compared to figure 8, which shows the magnitude of the second-order spatial derivative divided by the magnitude of the magnetic field.

3.3. Influence of a ferromagnetic disturbance

The influence of a ferromagnetic object on the measurements of the magnetic field is indicated in figure 9. The figure shows the percentage difference for the x and y directions between the disturbed and undisturbed magnetic fields with the sensor at a fixed position ($(x, y) = (0.3, 0.1)$ m), and varying positions of the ferromagnetic object (figure 3). The percentage difference at the location of the sensor due to the use of the linearized model for an uncertainty of 0.03 m in the x and y directions (figure 7) is indicated by the solid and dashed lines, respectively. From the figure it becomes clear that the measurements will be influenced only when the ferromagnetic object is located near or between the source and the sensor.

To analyze the effect of a ferromagnetic disturbance on the estimation of position and orientation, updates of the state and covariance were calculated in a disturbed and an undisturbed environment using (4). Assume the sensor to be located at position $\left(\hat{\boldsymbol{p}}_s^c = (0.3 \quad 0.1 \quad 0.0)^T \text{ m}\right)$ and an orientation aligned with the coil frame $\left(\hat{\mathbf{R}}_s^c = \mathbf{I}\right)$. The position and orientation errors are assumed to be 0.01 m and 0.01 rad, respectively, which means for the covariance matrix $\mathbf{P}_k^- = 0.01^2 \cdot \mathbf{I}$. The measurement noise is assumed to be uncorrelated, which means the covariance is given by $\mathbf{R}_v = \sigma_v^2 \cdot \mathbf{I}$. The percentage differences between the calculated update using the measurement with a ferromagnetic object between the source and the sensor ($\boldsymbol{p} = (0.1 \quad 0.1 \quad 0.0)^T$ m, figure 9) and the correct update (initial position and orientation error: $\delta\boldsymbol{x} = (0.01 \quad 0.01 \quad 0.01 \quad 0.01 \quad 0.01 \quad 0.01)^T$) were calculated to be 81% for the x direction, 47% for the y direction and 92% for the z direction. If the undisturbed measurement is

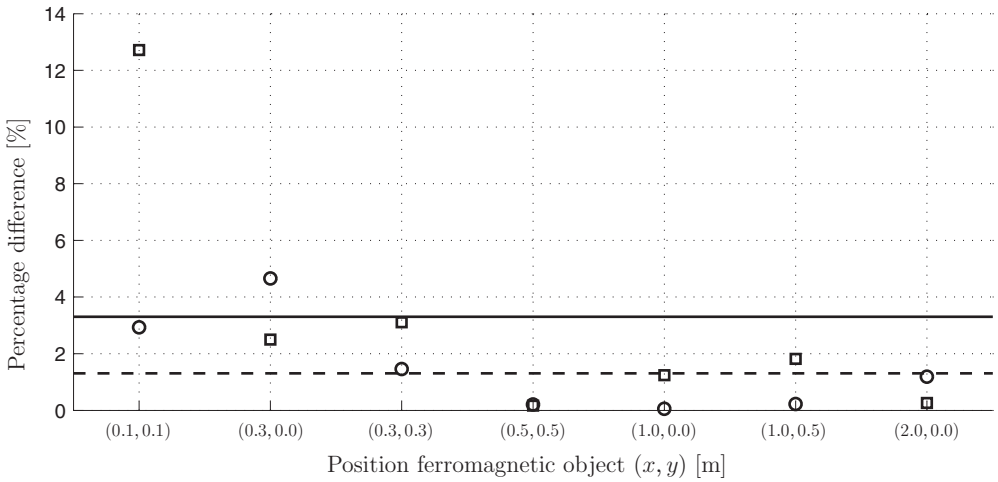

Figure 9. Percentage difference between the measured magnetic field (x circles, y squares) with ferromagnetic disturbance and the undisturbed field at sensor position $(x, y) = (0.3, 0.1)$ m, and varying position of the ferromagnetic object. The percentage difference due to the use of the linearized model at the position of the sensor with an uncertainty of 0.03 m is indicated by lines (x uncertainty solid, y uncertainty dashed).

used, the percentage differences were calculated to be 6%,18% and 6% for the x, y and z directions, respectively. Yet, the reduction of the covariance $\mathbf{P}_k$ is updated equally, yielding inconsistent behaviour of the filter in a disturbed environment.

4. Discussion

In this study, a stochastic measurement model is proposed that can be used in a fusion filter to estimate relative positions and orientations [18]. The model is used to predict the magnetic field generated by a single coil, measured by a remote 3D magnetic sensor, based on an estimation of the relative position and orientation of the remote sensor with respect to the source. The main advantage of this model is that it allows the filter to decide to actuate only when necessary, and to actuate only the coil with the largest contribution to the reduction of the uncertainty associated with the position and orientation estimation. The model is validated using a single coil in a 2D setup, which is sufficient since the magnetic field of a single coil is axial symmetric. Compared to existing models (e.g. [13]), the calculations are not based on the dipole approximation of the source and do not require the source coils to be mounted orthogonally or to share the same origin. The model is accurate, which is confirmed by the small rms differences between the predicted magnetic field and the measured magnetic field. When the dipole approximation is used, the errors increase as expected, especially for sensor locations near the source coil. The use of a linearized measurement model to update the state and the appearance of a ferromagnetic object in the vicinity of the source and the sensor were defined as two sources of error that may lead to divergence of the fusion filter. It appeared that the linearized model introduces errors which generally increase for sensor locations near the source. Moreover, it was shown that the errors are dependent on the second-order spatial derivative of the magnetic field. As expected [21, 22], it appeared that a ferromagnetic object influences the measurements only if it is located near or between the source and the sensor, making the system insensitive for most ferromagnetic objects in the environment. It was shown in section 3.3 that a ferromagnetic object in the vicinity of the sensor may lead to inconsistent behaviour of the fusion filter. It should be noted that a part of the error for both the disturbed and undisturbed cases is caused by the use of the linearized model. To prevent inconsistent behaviour of the filter, the filter should be updated regularly to limit the growth of the state uncertainty. Moreover, it is important to remove any ferromagnetic objects in the vicinity of the source or the sensor. Unlike heading estimation systems using the Earth's magnetic field [23], the proposed measurement system is insensitive to ferromagnetic objects in the environment outside the range of the configuration.

The disturbance due to a ferromagnetic object in the vicinity of the source or the sensor can be caused by two phenomena, eddy currents and ferromagnetism. Eddy currents are induced in conductive objects in the vicinity of the source or the sensor by a changing magnetic field, which occurs during the rising and falling edges of a magnetic pulse. After the pulse has reached its steady-state value, the eddy currents decay at an exponential rate with a time constant defined by the ratio between inductance and resistance of the object [19]. For the iron object used in the experiments, the time constant will be in the order of microseconds. This means that the eddy currents did not have a noticeable effect on the experiments performed in the present study, since the sample time was set to 10 ms. The magnetization field produced by ferromagnetic materials in the vicinity of the source or the sensor persists while the magnetic actuation is applied, where the magnitude of the magnetization field depends on the permeability of the material. This means that the disturbances presented in figure 9 can be attributed to ferromagnetism.

Figure 5 indicates that a large number of samples are preferable for accuracy, but must be kept small to limit the disturbance caused by movements during a pulse. The time needed to acquire enough samples can be decreased

by increasing the sample frequency of the magnetometers. However, as stated, eddy currents will be induced due to the rising and falling edge of a pulse, which will generate secondary magnetic fields in conducting objects near the source or the sensor. Before sampling at high frequency, some time should be allowed for the eddy currents to decay. When sampling at high frequency, the bandwidth of the magnetometer noise should be kept in mind to prevent correlation between measurement noise samples.

The measurement setup used in this study was able to generate constant (dc) magnetic fields only. It could be interesting to investigate the use of time varying (ac) magnetic fields. The main reason to use dc magnetic fields is that they are less sensitive to metallic object interference, since only the rising and falling edge of a pulse will generate eddy currents. AC magnetic fields offer the possibility of actuating multiple coils simultaneously while less energy is used. However, the changing magnetic field induces eddy currents continuously, which need to be taken into account. Moreover, the equations used to predict the magnetic field will become time dependent which increases the complexity. Still, from an energetic point of view, it is interesting to investigate the possibility of using ac magnetic fields.

The coil used for the experiments was a circular coil consisting of 50 windings which were assumed to be of infinitesimal thickness. In reality, however, each individual winding will have a certain thickness and the coil does not necessarily have to be in a perfect circular shape. This incorrect assumption introduces a systematic error into the system that will be different for each coil configuration. An improvement could be to model each individual coil by applying the Biot–Savart law [19], or by using a numerical lookup table for the magnetic field at each position and orientation. In principle, for the method proposed, any coil geometry can be used, as long as the mapping function $\boldsymbol{h}(\boldsymbol{x})$ and its partial derivatives are known. For human motion applications, the coils could be placed around body segments or integrated within clothes such that it does not impede normal functioning. Moreover, the dimensions of the coil (e.g. number of windings, coil radius) can be optimized with respect to the range that should be covered by that coil. Also, several coil radii or higher actuation currents can be used when large distances need to be covered. For a sufficient signal-to-noise ratio, the range of the coil used in the current setup is limited to about 80 cm.

The measurement model proposed in the present study was used in an adaptive filter structure using three source coils in a successive study [18]. The state variables, the position and orientation of the source and sensors, were estimated using the accelerometer and gyroscope signals of inertial sensors. The filter estimated the uncertainty associated with each state variable. If the uncertainty associated with one of the state variables exceeded a predefined threshold, the filter decided to perform a magnetic actuation using a single coil each time. The equations used to update the state (4) were used to choose the coil resulting in the largest reduction of the uncertainty. The average rms error was 0.033 m for the position and 3.6° for the orientation. Compared to another study [14], the proposed system showed lower accuracy for the relative position (position error approximately five times larger) and comparable accuracy for the relative orientation. Yet, significant improvements were achieved for the update rate, and pulse width using a Kalman filter running real time. Moreover, the filter used the stochastic model described in this study to decide when to actuate and to choose which coil to actuate. A system using this stochastic model is not based on a specific coil configuration allowing flexibility in the design of the system, and will show a reduction of the energy consumption due to minimal actuation.

Acknowledgments

This study was financially supported by the Dutch Ministry of Economic Affairs under the FreeMotion project.

References

[1] Roetenberg D, Luinge H J, Baten C T M and Veltink P H 2005 Compensation of magnetic disturbances improves inertial and magnetic sensing of human body segment orientation *IEEE Trans. Neural Syst. Rehabil. Eng.* **13** 395–405

[2] Luinge H J and Veltink P H 2005 Measuring orientation of human body segments using miniature gyroscopes and accelerometers *Medical Biol. Eng. Comput.* **43** 273–82

[3] Foxlin E 2005 Pedestrian tracking with shoe-mounted inertial sensors *IEEE Comput. Graph. Appl.* **25** 38–46

[4] Yun X and Bachmann E R 2006 Design, implementation and experimental results of a quaternion-based Kalman filter for human body motion tracking *IEEE Trans. Robot.* **22** 1216–27

[5] Schepers H M, Koopman H F J M and Veltink P H 2007 Ambulatory assessment of ankle and foot dynamics *IEEE Trans. Biomed. Eng.* **54** 895–902

[6] Sabatini A M, Martelloni C, Scapellato S and Cavallo F 2005 Assessment of walking features from foot inertial sensing *IEEE Trans. Biomed. Eng.* **52** 486–94

[7] Tan H, Wilson A M and Lowe J 2008 Measurement of stride parameters using a wearable GPS and inertial measurement unit *J. Biomech.* **41** 1398–406

[8] Caron F, Duflos E, Pomorski D and Vanheeghe P 2006 GPS/IMU data fusion using multisensor Kalman filtering: introduction of contextual aspects *Inform. Fusion* **7** 221–30

[9] Foxlin E, Harrington M and Pfeifer G 1998 Constellation: a wide range wireless motion-tracking system for augmented reality and virtual set applications *Proc. ACM SIGGRAPH Conf. on Computer Graphics (Orlando, FL, USA)* pp 371–8

[10] Roetenberg D and Veltink P H 2005 Camera-marker and inertial sensor fusion for improved motion tracking *Gait Posture* **22** 51–2

[11] Emura S and Tachi S 1998 Multisensor integrated prediction for virtual reality *Presence* **7** 410–22

[12] Tanigawa M, Hol J D, Dijkstra F, Luinge H J and Slycke P J 2008 Augmentation of low-cost GPS/MEMS INS with UWB positioning system for seamless outdoor/indoor positioning *ION GNSS volume Session C4: Indoor Positioning (Savannah, GA, USA)* pp 1–8

[13] Roetenberg D, Slycke P, Ventevogel A and Veltink P H 2007 A portable magnetic position and orientation tracker *Sensors Actuators* A **135** 426–32

[14] Roetenberg D, Slycke P and Veltink P H 2007 Ambulatory position and orientation tracking fusing magnetic and inertial sensing *IEEE Trans. Biomed. Eng.* **54** 883–90

[15] Kuipers J 1976 Tracking and determining orientation of object using coordinate transformation means, system and process *US Patent* 3,983,474

[16] Raab F H, Blood E B, Steiner T O and Jones H R 1979 Magnetic position and orientation tracking system *IEEE Trans. Aerosp. Electron. Syst.* **15** 709–18

[17] Paperno E, Sasada I and Leonovich E 2001 A new method for magnetic position and orientation tracking *IEEE Trans. Magn.* **37** 1938–40

[18] Schepers H M, Roetenberg D and Veltink P H 2010 Ambulatory human motion tracking by fusion of inertial and magnetic sensing with adaptive actuation *Med. Biol. Eng. Comput.* **48** 27–37

[19] Cheng D K 1989 *Field and Wave Electromagnetics* 2nd edn (Reading, MA: Addison-Wesley)

[20] Brown R G and Hwang P Y C 1997 *Introduction to Random Signals and Applied Kalman Filtering* 3rd edn (New York: Wiley)

[21] LaScalza S, Arico J and Hughes R 2003 Effect of metal and sampling rate on accuracy of Flock of Birds electromagnetic tracking system *J. Biomech.* **36** 141–4

[22] Nixon M A, McCallum B C, Fright W R and Price N B 1998 The effects of metals and interfering fields on electromagnetic trackers *Presence* **7** 204–18

[23] de Vries W H K, Veeger H E J, Baten C T M and van der Helm F C T 2009 Magnetic distortion in motion labs, implications for validating inertial magnetic sensors *Gait Posture* **29** 535–41